

An Auto-validating Rejection Sampler

Raazesh Sainudiin[†] and Thomas L. York^{*†}

[†]*Department of Mathematics and* ^{*}*Department of Biological Statistics and Computational Biology, Cornell University, Ithaca, U.S.A.*

Summary. In Bayesian statistical inference and computationally intensive frequentist inference, one is interested in obtaining samples from a high dimensional, and possibly multi-modal target density. The challenge is to obtain samples from this target without any knowledge of the normalizing constant. Several approaches to this problem rely on Monte Carlo methods. One of the simplest such methods is the rejection sampler due to von Neumann. Here we introduce an auto-validating version of the rejection sampler via interval analysis. We show that our rejection sampler does provide us with independent samples from a large class of target densities in a guaranteed manner. We illustrate the efficiency of the sampler by theory and by examples in up to 10 dimensions. Our sampler is immune to the ‘pathologies’ of some infamous densities including the witch’s hat and can rigorously draw samples from piece-wise Euclidean spaces of small phylogenetic trees.

1. INTRODUCTION

Obtaining samples from a density $p(\theta) \triangleq p^*(\theta)/N_p$, where $\theta \in \Theta$ and Θ is a compact Euclidean subset, *i.e.*, $\Theta \subset \mathbb{R}^n$, without any knowledge of the normalizing constant $N_p \triangleq \int_{\Theta} p^*(\theta) d\theta$, is a basic problem in Bayesian inference and multivariate simulation. Several approaches to this problem rely on computationally-intensive Monte Carlo methods through conventional floating-point arithmetic. We will concentrate on the rejection sampler due to von Neumann [43]. After a brief introduction to the rejection sampler (RS) in Section 2, an interval version of this sampler is formalized in Section 3. This sampler is referred to as the Moore rejection sampler (MRS) in honor of Ramon E. Moore who was one of the influential founders of interval analysis [34]. A brief introduction to interval analysis, a prerequisite to understanding MRS, as well as the notational conventions and background assumed in the rest of the paper, are given in Section 7 for readers who are new to interval methods. In Section 8, Lemma 1 shows that MRS produces independent samples from the desired target density and Lemma 2 describes the asymptotics of the acceptance probability for a refining family of MRSs. Examples demonstrating the robustness and efficiency of MRS to complexity and dimensionality of the target are discussed in Section 4. We conclude in Section 5. Our sampler is an adaptive and auto-validating von Neumann rejection sampler that can draw independent samples from a large class of target densities, including non-log-concave, sharp-peaked, and multi-modal targets. Unlike many conventional samplers, each sample produced by MRS is equivalent to a computer-assisted proof that it is drawn from the desired target. An open source C++ class library for MRS is publicly available from www.stats.ox.ac.uk/~sainudii/codes.

[†]*Address for correspondence:* current affiliation: Raazesh Sainudiin, Department of Statistics, 1 South parks Road, University of Oxford, Oxford OX1 3TG, U.K.
E-mail: sainudii@stats.ox.ac.uk

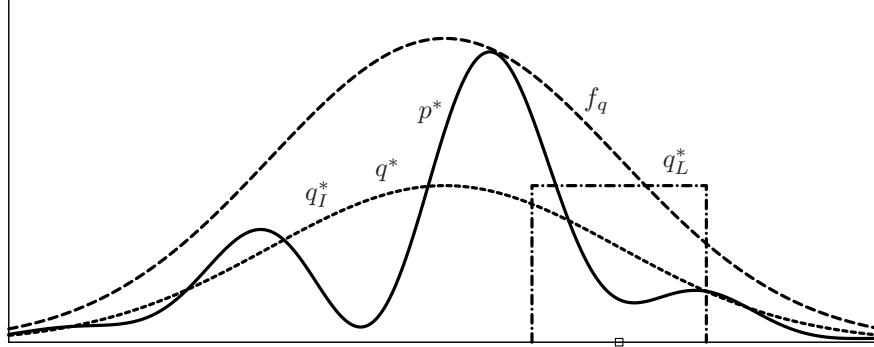


Fig. 1. The characteristics of three samplers with target $p = p^*/N_p$: (1) Rejection sampler with proposal $q = q^*/N_q$ and the envelope function f_q , (2) an independent Metropolis-Hastings sampler (IMHS) driven by an independent base chain I with proposal $q_I = q_I^*/N_{q_I^*}$ and (3) a local Metropolis-Hastings sampler (LMHS) driven by a local base chain L with proposal $q_L = q_L^*/N_{q_L^*}$ centered at the current state (open square at the bottom).

2. Rejection Sampler (RS)

Rejection sampling [43] is a Monte Carlo method to draw independent samples from a target probability distribution $p(\theta) \triangleq p^*(\theta)/N_p$, where $\theta \in \Theta \subset \mathbb{R}^n$. Typically the target p is any density that is absolutely continuous with respect to the Lebesgue measure. In most cases of interest we can compute the target shape $p^*(\theta)$ for any $\theta \in \Theta$, but the normalizing constant N_p is unknown. Given a proposal density $q = q^*/N_q$ and an envelope function f_q (Figure 1) over Θ that satisfy certain conditions, RS can produce samples from p as follows:

2.1. Rejection Sampling Algorithm

- (a) Choose a proposal density $q(\theta) = q^*(\theta)/N_q$ from which independent samples can be drawn, $N_q \triangleq \int_{\Theta} q^*(\theta) d\theta$ is known, and $q^*(\theta)$ is computable for any $\theta \in \Theta$.
- (b) Find some c for which the inequality

$$f_q(\theta) \triangleq cq^*(\theta) \geq p^*(\theta), \forall \theta \in \Theta \quad (1)$$

is satisfied. The smallest such value of c is said to be optimal and denoted by \hat{c} , i.e.,

$$\hat{c} \triangleq \inf\{c : cq^*(\theta) \geq p^*(\theta), \forall \theta \in \Theta\}.$$

- (c) Given (I) a target shape $p^*(\theta)$, (II) a proposal density $q(\theta)$, and (III) an envelope function $f_q(\theta)$, $\forall \theta \in \Theta$, that satisfy the above conditions, we can draw independent samples from the target $p(\theta)$ as follows:

- (i) GENERATE $T \sim q$.
- (ii) DRAW $H \sim \text{Uniform}[0, f_q(T)]$, where $f_q(T) \geq p^*(T)$.
- (iii) IF $H \leq p^*(T)$, THEN set $U = T$.

(iv) RETURN to Step ci.

It is not difficult to see that U generated by the above algorithm is distributed according to p [29, 45]. Observe that the probability $\mathbf{A}_{f_q}^p$ that a point proposed according to q gets accepted as an independent sample from p through the envelope function f_q is the ratio of the integrals

$$\mathbf{A}_{f_q}^p = \frac{N_p}{N_{f_q}} \triangleq \frac{\int_{\Theta} p^*(\theta) d\theta}{\int_{\Theta} f_q(\theta) d\theta},$$

and the probability distribution over the number of samples from q to obtain one sample from p is geometrically distributed with mean $1/\mathbf{A}_{f_q}^p$ [29, 45]. Therefore, for a given p , we have to minimize N_{f_q} over the allowed possibilities for q and f_q in order to obtain an efficient sampler with a high acceptance probability $\mathbf{A}_{f_q}^p$.

3. Moore Rejection Sampler (MRS)

Moore rejection sampler (MRS) is an auto-validating rejection sampler (RS). It can produce independent samples from any target shape p^* that has a well-defined natural interval extension P^* (Definition 5) over a compact domain Θ . MRS is said to be auto-validating because it automatically obtains a proposal q that is easy to simulate from, and an envelope f_q that is guaranteed to satisfy the envelope condition (1). MRS guarantees independent samples through auto-validating interval methods that also constitute the core of several recent computer-assisted proofs of challenging problems [26].

3.1. Theory

In summary, the defining characteristics and notations of MRS are:

Compact domain	$\Theta = [\underline{\theta}, \bar{\theta}]$
Target shape	$p^*(\theta) : \Theta \rightarrow \mathbb{R}$
Target integral	$N_p \triangleq \int_{\Theta} p^*(\theta) d\theta$
Target density	$p(\theta) \triangleq \frac{p^*(\theta)}{N_p} : \Theta \rightarrow \mathbb{R}$
Interval extension of p^*	$P^*(\Theta) : \mathbb{I}\Theta \rightarrow \mathbb{I}\mathbb{R}$
Proposal shape	$q^*(\theta) : \Theta \rightarrow \mathbb{R}$
Proposal integral	$N_q \triangleq \int_{\Theta} q^*(\theta) d\theta$
Proposal density	$q(\theta) \triangleq \frac{q^*(\theta)}{N_q} : \Theta \rightarrow \mathbb{R}$
Envelope function	$f_q(\theta) = cq^*(\theta)$
Envelope integral	$N_{f_q} \triangleq \int_{\Theta} f_q(\theta) d\theta = cN_q$
Acceptance probability	$\mathbf{A}_{f_q}^p = \frac{N_p}{N_{f_q}}$
Partition of Θ	$\mathfrak{T} := \{ \Theta^{(1)}, \Theta^{(2)}, \dots, \Theta^{(\mathfrak{T})} \}.$

If $p^* \in \mathfrak{E}$, the class of elementary functions (Definition 7), and its natural interval extension P^* is well-defined on Θ , then by Theorem 4

$$\text{Rng}(p^*; \Theta) \triangleq p^*(\Theta) \subseteq P^*(\Theta) \triangleq [\underline{P}^*(\Theta), \overline{P}^*(\Theta)]$$

which implies that

$$\underline{P}^*(\Theta) \leq p^*(\theta) \leq \overline{P}^*(\Theta), \forall \theta \in \Theta \quad (2)$$

Although $[\underline{P}^*(\Theta), \overline{P}^*(\Theta)]$ may over-estimate the range $p^*(\Theta)$, we can construct a naive MRS to draw samples from p by using the following uniform proposal and constant envelope in Algorithm 2.1.

$$\begin{aligned} q(\theta) &= \frac{\overline{P}^*(\Theta)}{d(\Theta) \cdot \overline{P}^*(\Theta)} = (d(\Theta))^{-1}, \text{ and} \\ f_q(\theta) &= \overline{P}^*(\Theta), \end{aligned}$$

where, $d(\Theta) = d([\underline{\theta}, \overline{\theta}]) = \overline{\theta} - \underline{\theta}$ is the *diameter* of Θ . A lower bound for the acceptance probability of this naive MRS is given by the range enclosure ratio:

$$\mathbf{A}_{\overline{P}^*(\Theta)}^p = \frac{N_p}{N_{\overline{P}^*(\Theta)}} = \frac{N_p}{d(\Theta) \cdot \overline{P}^*(\Theta)} \geq \frac{d(\Theta) \cdot \underline{P}^*(\Theta)}{d(\Theta) \cdot \overline{P}^*(\Theta)} = \frac{\underline{P}^*(\Theta)}{\overline{P}^*(\Theta)}.$$

Although this naive MRS can be extremely inefficient (i.e., can have a very low acceptance probability) for non-constant target shapes, one has the guarantee due to (2) that the necessary envelope condition (1) is satisfied.

A natural way to improve efficiency (i.e., increase the acceptance probability) is via partitions. Let $\mathfrak{T} \triangleq \{\Theta^{(1)}, \Theta^{(2)}, \dots, \Theta^{(|\mathfrak{T}|)}\}$ be a finite partition of Θ . Then by Theorem 4 we can enclose $p^*(\Theta^{(i)})$, the range of p^* over the i -th element of \mathfrak{T} , with the well-defined interval extension P^* of p^* over Θ

$$p^*(\Theta^{(i)}) \subseteq P^*(\Theta^{(i)}) \triangleq [\underline{P}^*(\Theta^{(i)}), \overline{P}^*(\Theta^{(i)})], \forall i \in \{1, 2, \dots, |\mathfrak{T}|\}. \quad (3)$$

For the given partition \mathfrak{T} we can construct a partition-specific proposal $q^{\mathfrak{T}}(\theta)$ as a normalized simple function over Θ ,

$$q^{\mathfrak{T}}(\theta) = (N_{q^{\mathfrak{T}}})^{-1} \sum_{i=1}^{|\mathfrak{T}|} \overline{P}^*(\Theta^{(i)}) \mathbf{1}_{\{\theta \in \Theta^{(i)}\}}, \quad (4)$$

where the normalizing constant is obtained from the sum

$$N_{q^{\mathfrak{T}}} \triangleq \sum_{i=1}^{|\mathfrak{T}|} \left(d(\Theta^{(i)}) \cdot \overline{P}^*(\Theta^{(i)}) \right).$$

The next ingredient $f_{q^{\mathfrak{T}}}(\theta)$ for our rejection sampler can simply be

$$f_{q^{\mathfrak{T}}}(\theta) = \sum_{i=1}^{|\mathfrak{T}|} \overline{P}^*(\Theta^{(i)}) \mathbf{1}_{\{\theta \in \Theta^{(i)}\}} \quad (5)$$

The necessary envelope condition (1) is satisfied by $f_{q^{\mathfrak{T}}}(\theta)$ because of (3). Now, we have all the ingredients to perform a more efficient partition-specific Moore rejection sampling. Lemma 1 shows that if the target shape p^* has a well-defined natural interval extension P^* , and if U is generated according to the steps in part c of Algorithm 2.1, and if the proposal density $q^{\mathfrak{T}}(\theta)$ and the envelope function $f_{q^{\mathfrak{T}}}(\theta)$ are given by (4) and (5), respectively, then U is distributed according to the target p . Note that the above arguments as well as those in the proof of Lemma 1 naturally extend when $\Theta \subset \mathbb{R}^n$ for $n > 1$. In the multivariate case, $\Theta^{(i)} \in \mathbb{IR}^n$ (Definition 3) is a box. Thus, we naturally replace the diameter of an interval by the *volume* of a box $v(\Theta^{(i)}) \triangleq \prod_{k=1}^n d(\Theta_k^i)$. The envelopes and proposals are now simple functions over a partition of the domain into boxes. Analogous to the univariate case, the

accepted samples are uniformly distributed in the region $S \subset \mathbb{R}^{n+1}$ ‘under’ p^* and ‘over’ Θ . Hence their density is p [45].

Next we bound the acceptance probability $\mathbf{A}_{f_{q^{\mathfrak{T}}}}^p \triangleq \mathbf{A}_{\mathfrak{T}}^p$ for this sampler. Due to the linearity of the integral operator and (3),

$$\begin{aligned} N_p &\triangleq \int_{\Theta} p^*(\theta) d\theta \\ &= \sum_{i=1}^{|\mathfrak{T}|} \int_{\Theta^{(i)}} p^*(\theta) d\theta \\ &\in \sum_{i=1}^{|\mathfrak{T}|} (d(\Theta^{(i)}) \cdot P^*(\Theta^{(i)})) \\ &= [\sum_{i=1}^{|\mathfrak{T}|} (d(\Theta^{(i)}) \cdot \underline{P}^*(\Theta^{(i)})), \sum_{i=1}^{|\mathfrak{T}|} (d(\Theta^{(i)}) \cdot \overline{P}^*(\Theta^{(i)}))]. \end{aligned}$$

Therefore,

$$\mathbf{A}_{\mathfrak{T}}^p = \frac{N_p}{N_{f_{q^{\mathfrak{T}}}}} = \frac{N_p}{\sum_{i=1}^{|\mathfrak{T}|} (d(\Theta^{(i)}) \cdot \overline{P}^*(\Theta^{(i)}))} \geq \frac{\sum_{i=1}^{|\mathfrak{T}|} (d(\Theta^{(i)}) \cdot \underline{P}^*(\Theta^{(i)}))}{\sum_{i=1}^{|\mathfrak{T}|} (d(\Theta^{(i)}) \cdot \overline{P}^*(\Theta^{(i)}))}.$$

We can say something more about the lower bound for $\mathbf{A}_{\mathfrak{T}}^p$ by limiting ourselves to target shapes within $\mathfrak{E}_{\mathcal{L}}$, the Lipschitz class of elementary functions (Definition 9). If $p^* \in \mathfrak{E}_{\mathcal{L}}$ then we might expect the enclosure of N_p to be proportional to the mesh w of the partition \mathfrak{T} ,

$$w \triangleq \max_{i \in \{1, \dots, \mathfrak{T}\}} d(\Theta^{(i)}).$$

Lemma 2 shows that if $p^* \in \mathfrak{E}_{\mathcal{L}}$ and \mathfrak{U}_W is a uniform partition of Θ into W intervals, then the acceptance probability $\mathbf{A}_{\mathfrak{U}_W}^p = 1 - \mathcal{O}(1/W)$. More generally, any family of MRSs that construct their envelopes with \overline{P}^* from the invoking family of refining partitions

$$\{ \mathfrak{T}_{\alpha} : \alpha \in \mathcal{A} \}$$

can be thought of as a family of rejection samplers whose envelopes descend from above on p^* in the form of simple functions. The acceptance probability approaches 1 at a rate that is no slower than linearly with the mesh. We can gain geometric insight into the sampler from an example. The dashed lines of a given shade, depicting a simple function in Figure 12, is a partition-specific envelope function (5) for the target shape $s^*(x) = -\sum_{k=1}^5 k x \sin(\frac{k(x-3)}{3})$ over the domain $\Theta = [-10, 6]$ and its normalization gives the corresponding proposal function (4). As the refinement of Θ proceeds through uniform bisections, the partition size increases as 2^i , $i = 1, 2, 3, 4$. Each of the corresponding envelope functions in increasing shades of gray can be used to draw auto-validated samples from the target $s(x)$ over Θ . Note how the acceptance probability increases with refinement.

3.2. Practice

We theoretically studied the efficiency of uniform partitions for their tractability. In practice, we may further increase the acceptance probability for a given partition size by adaptively partitioning Θ . In our context, adaptive means the possible exploitation of any current information about the target. We can refine the current partition \mathfrak{T}_{α} and obtain a finer partition $\mathfrak{T}_{\alpha'}$ with an additional box by bisecting a box $\Theta^{(*)} \in \mathfrak{T}_{\alpha}$ along the side with the maximal diameter. There are several ways to choose a $\Theta^{(*)} \in \mathfrak{T}_{\alpha}$ for bisection. We explore three ways of choosing $\Theta^{(*)}$ from the current partition: (a) the box with the

largest volume, (b) the box with the largest diameter for its range enclosure and (c) the box with the largest diameter for the product of its volume and its range enclosure. When $\Theta^{(i)} \in \mathbb{I}\mathbb{R}^n$ with volume $v(\Theta^{(i)})$, the three schemes can be formalized as follows:

$$\begin{aligned}
 (a) \text{ Volume-based} \quad & \Theta^{(*)} = \arg \max_{\Theta^{(i)} \in \mathfrak{T}_\alpha} v(\Theta^{(i)}) \\
 (b) \text{ Range-based} \quad & \Theta^{(*)} = \arg \max_{\Theta^{(i)} \in \mathfrak{T}_\alpha} d(P^*(\Theta^{(i)})) \\
 (c) \text{ Integral-based} \quad & \Theta^{(*)} = \arg \max_{\Theta^{(i)} \in \mathfrak{T}_\alpha} \left(v(\Theta^{(i)}) \cdot d(P^*(\Theta^{(i)})) \right)
 \end{aligned} \tag{6}$$

Given a partitioning scheme, we employ a priority queue to conduct sequential refinements of Θ . This approach avoids the exhaustive $\arg \max$ computations to obtain the $\Theta^{(*)}$ for bisection at each refinement step. A priority queue (PQ) is a container in which the elements may have different user-specified priorities. The priority is based on some sorting criterion that is applicable to the elements in the container. The PQ can be thought of as a collection in which the “next” element is always the one with the highest priority, i.e., the largest with respect to the specified sorting criterion. Since this container sorts using a *heap* which can be thought of as a binary tree, one can add or remove elements in logarithmic time. This is a desirable feature of the PQ. We implement the above three refinement schemes through PQs based on their respective sorting criterion. The (a) the volume-based PQ manages the family of partitions \mathfrak{U}_W , (b) the range-based PQ manages the family \mathfrak{R}_α and (c) the integral-based PQ manages the family \mathfrak{V}_α .

Once we have any partition \mathfrak{T} of Θ , we can efficiently sample $\theta \sim q^{\mathfrak{T}}$ given by (4) in two steps. First we sample a box $\Theta^{(i)} \in \mathfrak{T}$ according to the discrete distribution $t(\Theta^{(i)})$,

$$t(\Theta^{(i)}) = \frac{v(\Theta^{(i)}) \cdot \overline{P}^*(\Theta^{(i)})}{\sum_{i=1}^{|\mathfrak{T}|} v(\Theta^{(i)}) \cdot \overline{P}^*(\Theta^{(i)})}, \quad \Theta^{(i)} \in \mathfrak{T}, \tag{7}$$

and then we choose a $\theta \in \Theta^{(i)}$ uniformly at random. Sampling from large discrete distributions (with million states or more) can be made faster by preprocessing the probabilities and saving the result in some convenient lookup table. This basic idea [30] allows samples to be drawn rapidly. We employ a more efficient preprocessing strategy [44] that allows samples to be drawn in constant time even for very large discrete distributions as implemented in the GNU Scientific Library [10]. Thus, by means of priority queues and lookup tables we can efficiently manage our adaptive partitioning of the domain for envelope construction, and rapidly draw samples from the proposal distribution. We used the Mersenne Twister random number generator [32] in this paper. Our sampler class builds on `C-XSC 2.0`, a C++ class library for extended scientific computing using interval methods [21]. All computations were done on a 2.8 GHz Pentium IV machine with 1GB RAM. Having given theoretical and practical considerations to our Moore rejection sampler, we are ready to draw samples from various targets.

4. Discussion with Examples

We empirically study sampler efficiency by sampling from qualitatively diverse targets since analytical results on efficiency are sharp only for relatively simple target parameterizations. In Section 4.1 we first study the relative efficiencies of MRSs managed by the three PQs

Table 1. Moore rejection sampling from six different Gaussian mixture target shapes g_n truncated over Θ , where n is the number of mixture components.

Target	Θ	Parameters
$g_1(x)$	$[-10^2, 10^2]$	$\mu_1 = -5, \sigma_1 = 1$, and $w_1 = 1.00$
$g_2(x)$	$[-10^2, 10^2]$	$\mu_1 = -5, \sigma_1 = 1, w_1 = 0.25, \mu_2 = 50,$ $\sigma_2 = 0.25$
$g_5(x)$	$[-10^2, 10^2]$	$\mu_1 = -15, \mu_2 = -5, \mu_3 = 3, \mu_4 = 6, \mu_5 = 50,$ $\sigma_1 = \sigma_2 = \sigma_4 = 1, \sigma_3 = 0.5, \sigma_5 = 0.1,$ $w_1 = 0.15, w_2 = 0.2, w_3 = 0.05, w_4 = 0.1$
$g'_5(x)$	$[-10^2, 10^2]$	same as $g_5(x)$, except $\sigma_1 = \sigma_2 = \sigma_4 = 0.1, \sigma_3 = 0.05, \sigma_5 = 0.01$
$g''_5(x)$	$[-10^2, 10^2]$	same as $g_5(x)$, except $\sigma_1 = \sigma_2 = \sigma_4 = 0.01,$ $\sigma_3 = 0.005, \sigma_5 = 0.001$
$\hat{g}_5(x)$	$[-10^{100}, 10^{100}]$	same as $g_5(x)$

(6) by sampling from univariate Gaussian mixture targets. Next, we study the effects of target complexity (number of components, scales and domain size) on sampler efficiency. In Section 4.2 we study the sampler behavior for a highly multi-modal two-dimensional target that is sensitive to a temperature parameter. Using a trivariate mixture target in Section 4.3, we compare MRS to Monte Carlo Markov chain (MCMC) methods that rely on heuristic convergence diagnostics and exploit the connections between RS, importance sampler (IS) and independent Metropolis-Hastings sampler (IMHS) to simultaneously produce samples from all of them. The effect of dimensionality on sampler efficiency is studied in Section 4.4 where we draw samples from multivariate targets, including the multivariate witch’s hat. Section 4.5 extends the sampler to piece-wise Euclidean domains of tree spaces. Here we draw auto-validating samples of small trees (triplets and quartets) from the target likelihood function based on primate molecular sequence data.

4.1. Univariate Gaussian Mixture

We apply MRS to targets whose shape g_n is obtained from finite mixtures of n univariate Gaussian densities truncated over an interval Θ . The means (μ_i ’s), standard deviations (σ_i ’s), weights (w_i ’s), and domains (Θ ’s) for each of the six targets studied are shown in Table 1.

First, we study the efficiency of the three partitioning schemes (6) by Moore rejection sampling from g_5 . Figure 2 shows the empirical acceptance probability of MRS, calculated from up to 10,000 draws from a maximum of 100,000 trials, at each partition size $|\mathcal{T}_\alpha|$ for each of the three different families of partitions ($\mathcal{U}_W, \mathcal{R}_\alpha$ and \mathcal{V}_α). Thus, for a given partition size $|\mathcal{T}_\alpha|$, the domain interval Θ gets adaptively partitioned through $|\mathcal{T}_\alpha| - 1$ bisections by the appropriate PQ. The family of partitions \mathcal{V}_α managed by the integral-based PQ is the most efficient as it can direct the next refining bisection towards the interval with the most uncertainty in its integral estimate. The efficiency of the integral-based scheme is even more pronounced for multivariate exponential mixtures (results not shown).

Note that Lemmas 1 and 2 guarantee that MRS produces independent draws from any target in $\mathfrak{E}_\mathfrak{d}$. This includes Gaussian mixture targets with any finite number of components truncated over any compact interval. Furthermore, the locations inside Θ are arbitrary and

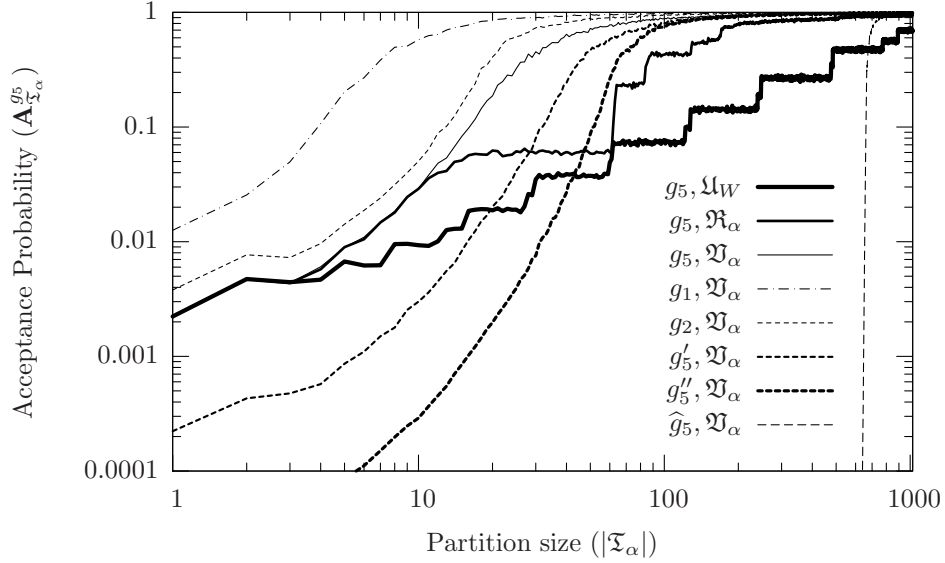


Fig. 2. Acceptance probability ($A_{\mathfrak{X}_\alpha}^p$) versus partition size ($|\mathfrak{X}_\alpha|$) for six target shapes $p^* = g_1, g_2, g_5, g'_5, g''_5, \widehat{g}_5$ (Table 1) under different families of partitions: (1) volume-based \mathfrak{U}_W , (2) range-based \mathfrak{R}_α and (3) integral-based \mathfrak{V}_α (see text for description).

the scales can be highly spiked (i.e., provided $\sigma_i > 0$ and can be enclosed by a machine interval via directed rounding [19, 25]). However, the efficiency of the sampler can depend on (i) number of components, (ii) spikiness of peaks and (iii) domain size. We empirically study these effects by sampling from the six targets (Table 1) using the family of MRSs induced by the most efficient partitions \mathfrak{V}_α . The acceptance probability plots (Figure 2) for targets g_1, g_2 , and g_5 illustrate the diminishing effect of the number of components on efficiency and those for targets g_5, g'_5 and g''_5 , with progressively smaller variances, illustrate a similar effect of spikiness on efficiency at every partition size $|\mathfrak{V}_\alpha|$. Note that in both cases sampler efficiency quickly recovers for larger partition sizes (> 100). Next we study the effect of domain size. In a computer, we cannot represent the real line and are forced to approximate it with the entire number screen, a compact interval. Thus, the domain of any target is necessarily truncated in a machine. The acceptance probability plot for the target shape \widehat{g}_5 , that is obtained by extending the domain of g_5 to a large interval of radius 10^{100} centered at 0, shows the effect of domain size. The first 700 bisections or so are spent on zoning in on the intervals with relatively higher probability mass. However, by 1000 bisections our acceptance probability is almost 1.

4.2. Bivariate Levy

The bivariate Levy density $l_T(X_1, X_2)$ over $\Theta \triangleq (\Theta_1, \Theta_2)' = [-100, 100]^{\otimes 2}$ (8) with temperature parameter T and normalizing constant N_{l_T} has 700 modes. Figure 3 shows l_{40}^* , i.e., the shape of the Levy density when $T = 40$ and 10,000 samples drawn from l_{40} using the MRS induced by an integral-based adaptive partitioning of the domain into 150 rectangles. This MRS produced 10,000 independent samples in less than 10 CPU seconds

at an acceptance probability of about 0.01. Mixtures of bivariate Gaussian shapes yielded comparable results.

$$l_T(X_1, X_2) = \frac{1}{N_{l_T}} l_T^*, \text{ where, } l_T^* = \exp\{-E(X_1, X_2)/T\}, \quad (8)$$

$$E(X_1, X_2) = \sum_{i=1}^5 i \cos((i-1)X_1 + i) \sum_{j=1}^5 j \cos((j+1)X_2 + j) \\ + (X_1 + 1.42513)^2 + (X_2 + 0.80032)^2.$$

As the temperature parameter T in l_T increases, the density approaches a uniform distribution on Θ . The density is more peaked at low values of T . Various MCMC methods that use local proposals tend to mix well at higher temperatures and get trapped at local peaks when T is small. To study the effect of temperature on our sampler's efficiency, we plot the empirical acceptance probability as well as the CPU seconds taken to draw 10,000 samples from each of four Levy targets at different temperatures ($T = 1, 4, 40, 400$) as a function of the partition size $|\mathfrak{A}_\alpha|$ (Figure 4). The efficiency decreases as the temperature cools. However, across the range of T we explored, MRS can produce 10,000 independent samples from l_T in a guaranteed manner within 10 CPU seconds with an acceptance probability greater than 1/100. Note that it is difficult to get a Monte Carlo Markov chain to mix properly and even more difficult to prove convergence for such targets.

4.3. Trivariate Needle in the Haystack

Using the target shape h^* (9) over $\Theta = [-10, 10]^{\otimes 3}$, we compare MRS to a popular MCMC sampler that relies on heuristics for convergence diagnosis and exploit the connection between three Monte Carlo methods. We begin with an introduction to an MCMC sampler known as the Metropolis-Hastings sampler (MHS) [33, 20] and a commonly used statistic for convergence diagnosis.

$$h^*(x) = \frac{1}{\sigma_1^3} \exp\{-\frac{1}{2}((x - \mu_1)/\sigma_1)^2\} + \frac{1}{\sigma_2^3} \exp\{-\frac{1}{2}((x - \mu_2)/\sigma_2)^2\} \quad (9)$$

4.3.1. Metropolis-Hastings Sampler and Convergence Diagnostics

Given $q_Y(\theta, \cdot)$, a possibly dependent proposal distribution for the base Markov chain Y (Figure 1), the following algorithm produces a Markov chain known as the Metropolis-Hastings (MH) chain on Θ merely from the knowledge of ratios of the form $p^*(\theta)/p^*(\theta')$ for any $(\theta, \theta') \in \Theta \times \Theta$. The stationary distribution of the MH chain is p .

- 1 Choose an arbitrary starting point θ_0 and set $i = 0$.
- 2 Generate a candidate point $\theta' \sim q_Y(\theta_i, \cdot)$ and $u \sim U(0, 1)$.
- 3 Set:

$$\theta_{i+1} = \begin{cases} \theta' & \text{if } u \leq \frac{p^*(\theta')q_Y(\theta', \theta_i)}{p^*(\theta_i)q_Y(\theta_i, \theta')} \\ \theta_i & \text{otherwise} \end{cases}$$
- 4 Set $i = i + 1$ and GO TO 2

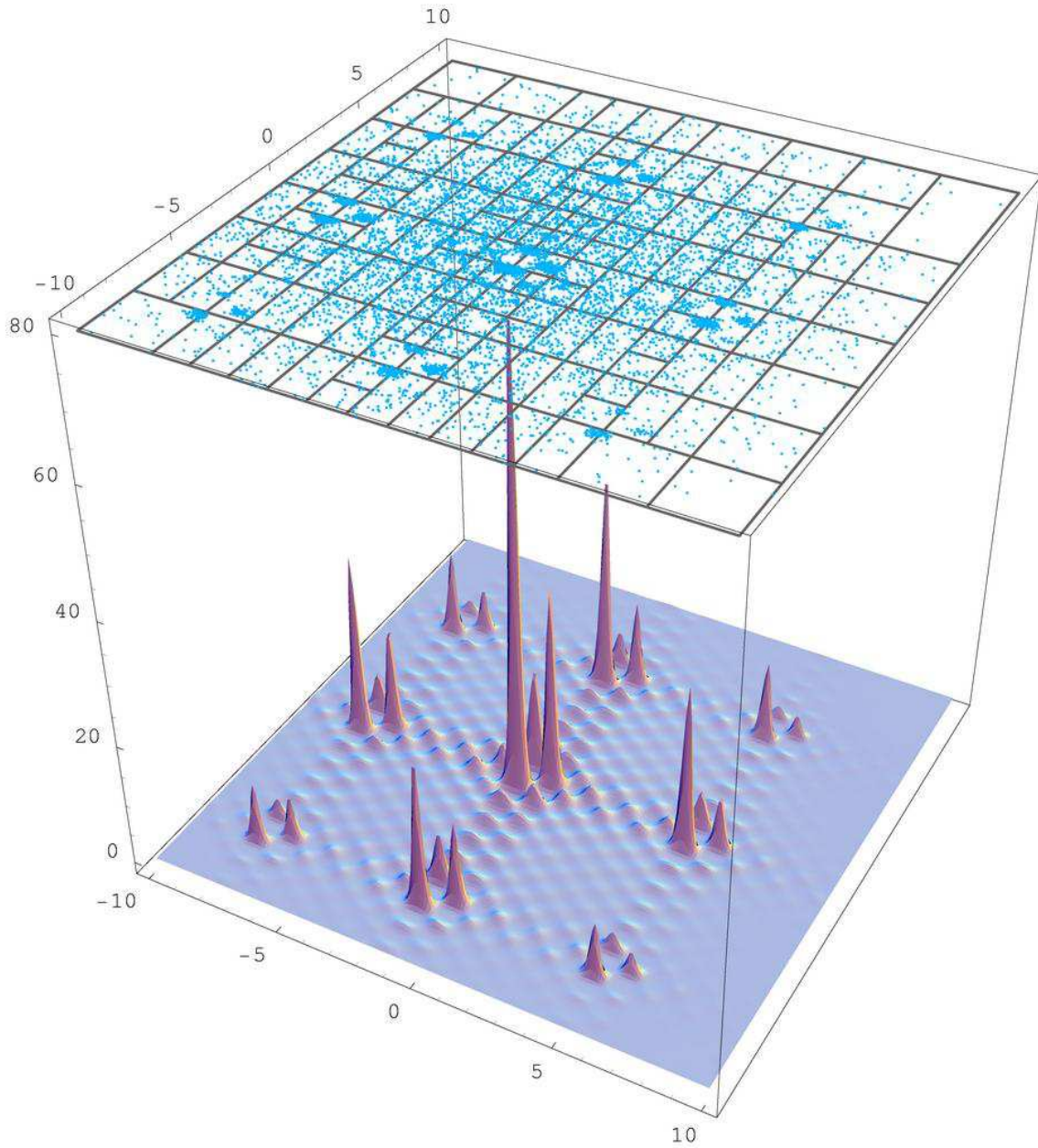


Fig. 3. Shape of the Levy density l_{40}^* with its 700 modes (8). 10,000 samples (points on top) from l_{40} using the MRS induced by an adaptive partitioning of the domain into 150 rectangles (with gray boundaries).

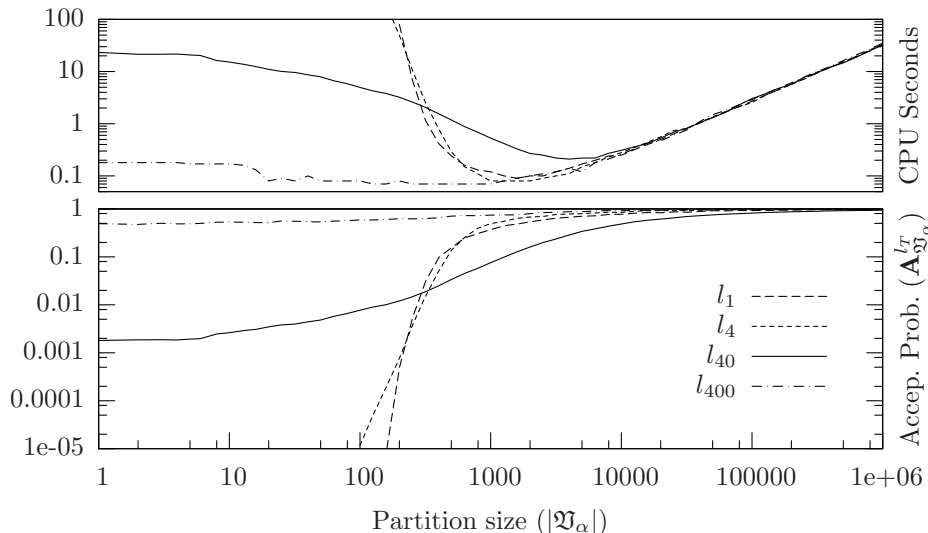


Fig. 4. Acceptance probability ($\mathbf{A}_{\mathfrak{V}_\alpha}^{l_T}$) and CPU seconds versus partition size ($|\mathfrak{V}_\alpha|$) for Levy targets l_T , where T is the temperature (8).

When the base chain has an independent proposal we refer to the MH chain it drives according to the above algorithm as the independent Metropolis-Hastings sampler (IMHS) and when the base chain has a local proposal we refer to the corresponding MH chain as the local Metropolis-Hastings sampler (LMHS).

Although the MH chain asymptotically approaches p , it is not trivial to know if it has converged even for relatively simple cases [7]. One often resorts to some heuristic convergence diagnostics. A fairly popular diagnostic statistic [13, 12] runs multiple MH chains with randomly dispersed initial conditions and compares the within (W) and between (B) chain variation of the sampled draws. When the ratio B/W is small enough, one can be fairly certain that all the chains have converged to the same distribution. Note that B/W in our definition is a unit translation of the statistic $\widehat{R} = 1 + B/W$, as defined in [12].

We run a MH chain with local proposal specified by a uniform cube of side $6\sigma_1$ centered at the current state. Using this LMHS we try to draw samples from the following needle in the haystack, i.e., h with the following parameters:

$$\mu_1 = (0, 0, 0)', \mu_2 = (1, 1, 1)', \sigma_1 = 1, \sigma_2 = 0.006. \quad (10)$$

To diagnose convergence of the LMHS we calculate B/W for each component of x and assume that the chain's burn-in time (the time when the samples may be affected by the initial condition) has ended when $B/W \leq 0.05$ for all three components. The post burn-in run length, i.e., the number of samples kept after the burn-in, is set to be 100 times the burn-in time (typical run lengths ranged in [10000, 50000] for target h specified by (10)).

The above convergence diagnostics are more conservative than the standard recommendations [13, 12, 24]. Figure 5 shows the results (along the x_1 axis) of the above LMHS that relies on the B/W statistic from four randomly initialized chains. The running mean for each of the four chains has converged to the haystack mean of $(0, 0, 0)'$ and completely

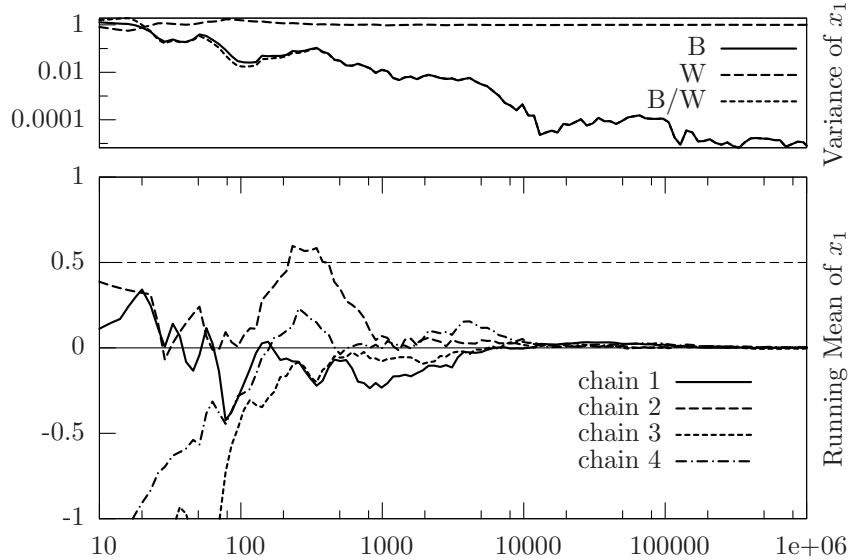


Fig. 5. The running mean for four MH chains, as well as B , W , and B/W for x_1 as a function of run length. The true mean for x_1 is at 0.5.

missed the needle at $(1, 1, 1)'$. Thus, if we relied on our convergence diagnostic B/W , which appears to be consistently vanishing and thus suggestive of convergence to our target h , we would have entirely missed the needle. Tuning the diagnostic parameters, including the number of chains, burn-in time, and run length, does not help diagnose true convergence for much sharper needles ($\sigma_2 < 10^{-5}$) that are naturally amenable to our MRS.

Next we compare the samples obtained from the B/W diagnosed LMHS described above with 10,000 samples from MRS induced by an integral-based adaptive partitioning of Θ into 1,000 boxes. We compare the two samplers on two targets: (1) a blunt needle with $\sigma_2 = 0.10$ and (2) a sharp needle with $\sigma_2 = 0.01$. The other parameters of the two targets are the same as before (10). The results are summarized in Figure 6. The diagnostic B/W works better in diagnosing convergence to the blunt target. The bias is severe for the sharp needle in all 100 replicates. MRS clearly outperforms LMHS, both in terms of producing the true samples and in terms of CPU time (Figure 6). Moreover, the sharpness of the needle only has a minor effect on the efficiency of MRS. For example, for a much sharper needle with $\sigma_2 = 10^{-10}$, the MRS induced by an integral-based adaptive partitioning of Θ into just 120 cuboids, achieves an acceptance probability of 0.40.

4.3.2. Rejection, Importance and Independent Metropolis-Hastings

The same proposal density used in RS may be used as the proposal in importance sampler (IS) [23, 31] or as the proposal of the independent base chain in IMHS. The latter two samplers are typically more efficient than RS, although in some cases the efficiency of IMHS can be as low as half that of RS [28]. The disadvantage of IMHS and IS (or RS) compared to MRS is in terms of diagnosing convergence and finding the right proposal(s), respectively. However, if one shares the proposal obtained through interval methods in MRS

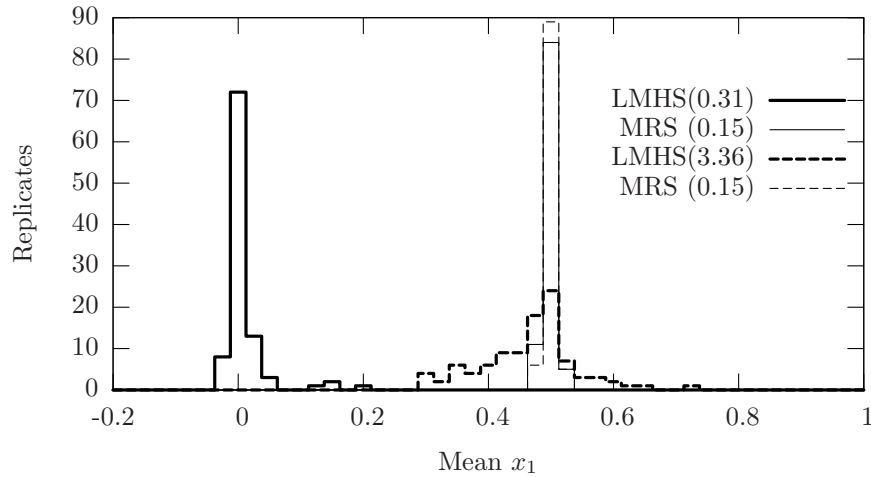


Fig. 6. Histograms of the mean x_1 from 100 replicates of the LMHS and MRS. The broken lines and solid lines represent targets with a blunt needle ($\sigma_2 = 0.10$) and a sharp needle ($\sigma_2 = 0.01$), respectively. The CPU time in seconds for each sampler is given in parenthesis.

with IS and IMHS, then we get their Moore versions which circumvent the disadvantages that arise from non-rigorously constructed proposals. Indeed all three samples may be generated simultaneously from the same sequence of proposed values [4]; each proposed value would be output with its importance weight, with some subset of the proposed values marked as IMHS-accepted, and with some further subset of those additionally marked as MRS-accepted and thereby constituting our collection of independent samples.

Figure 7 shows the mean squared error MSE for the sampler trio as a function of the size of the partition that is invoking their common proposal. The sample trio is drawn from our target h (9) with the sharp needle ($\sigma_2 = 0.01$). To obtain the MSE for each sampler with target p and proposal q , we drew $x_i \sim q$, $i = 1, \dots, N$ using MRS, where N is the number of samples needed to obtain 100 Moore rejection samples. For IS each of the x_i 's were assigned the importance sampling weight $w_i = p(x_i)/q(x_i)$ and the estimated mean $\hat{\mu} = \sum_{i=1}^N (w_i x_i) / \sum_{i=1}^N w_i$. The MRS estimated mean is $\hat{\mu} = \sum_{i=1}^{100} x_{r_i} / 100$, where x_{r_i} is the i^{th} MRS sample. For IMHS the mean is estimated by $\hat{\mu} = \sum_{i=r_1}^N x_i / (N - r_1 + 1)$, where r_1 is the index of the first MRS sample; the early samples x_i , $i < r_1$ are excluded as burn-in. This mean estimation was repeated 500 times to obtain $\hat{\mu}_j$, $j = 1, \dots, 500$ for each sampler. Finally, the MSE was computed with the known mean $\mu = (0.5, 0.5, 0.5)$ under the Euclidean norm $\|\hat{\mu}_j - \mu\|$ as $\sum_j \|\hat{\mu}_j - \mu\|^2 / 500$.

The Figure 7 compares the three samplers and shows a typical pattern: at low acceptance probability, IS has lowest MSE, and MRS the highest, while at high acceptance probability all three samplers approach the same MSE. The lower MSE of IS is due to the large number of (MRS-discarded) samples being appropriately weighted. Observe that such an auto-validating Moore importance sampler can be efficient and rigorous in estimating some expectation $E_p f(x)$ of interest. As the acceptance probability of MRS increases with refinement of the domain and the number of samples from each sampler approaches equality, the MSE of all three samplers converge as expected. For some target shapes, e.g. the

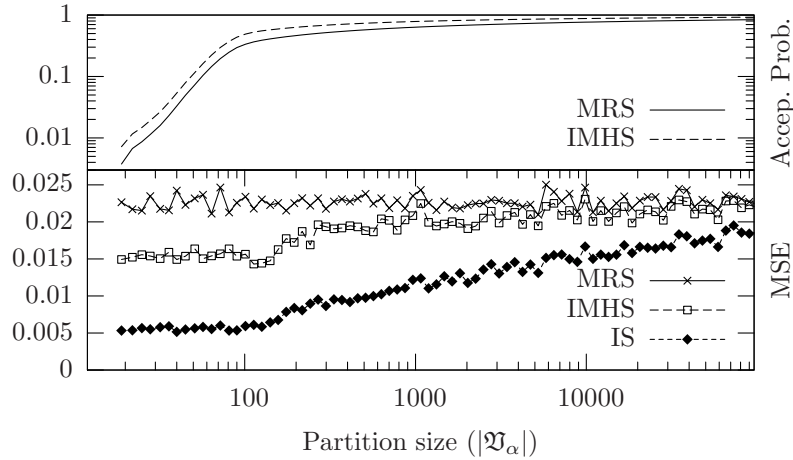


Fig. 7. MSE of the three samplers, namely, MRS, IMHS and IS, as well as the acceptance probability of MRS and IMHS as a function of partition size (see text for description).

witches hat (12), we have observed the MSE of IMHS to be greater than that of MRS, but by less than a factor of 2, in agreement with [28] (results not shown).

4.4. Multivariate Rosenbrock and Witch's Hat

Next we examine the effect of dimensionality on efficiency of MRS through the challenging Rosenbrock function from the optimization literature. We make it a Rosenbrock density (r_D) in D dimensions over some compact $\Theta \in \mathbb{R}^D$ by appropriately normalizing the Rosenbrock shape r_D^* (11).

$$r_D^*(X) = \exp\left\{-\sum_{i=2}^D (100(X_i - X_{i-1}^2)^2 + (1 - X_{i-1})^2)\right\} \quad (11)$$

Figure 8 summarizes the efficiency for various Rosenbrock densities. For the more demanding nine dimensional Rosenbrock target r_9 , we were able to draw 10,000 samples in about 650 CPU seconds at an acceptance probability of 1/10,000. The acceptance probability can be improved and/or D can be increased naively if we allowed the partition size to be greater than a million. Thus, the extent of RAM (random access memory) at our disposal ultimately determines the complexity and dimensionality of the target that can be rigorously sampled with MRS. However, the manner in which the natural interval extension is constructed will greatly affect the sampler's efficiency as discussed later. The acceptance probability for the relatively less complicated multivariate exponential mixture density truncated over $\Theta = [-100, 100]^{\otimes 10}$ is higher at 1/1000 compared to that for the Rosenbrock target r_9 even when there were 10 modes inside a 10-dimensional Θ (results not shown). Thus, the complexity of the target greatly affects efficiency.

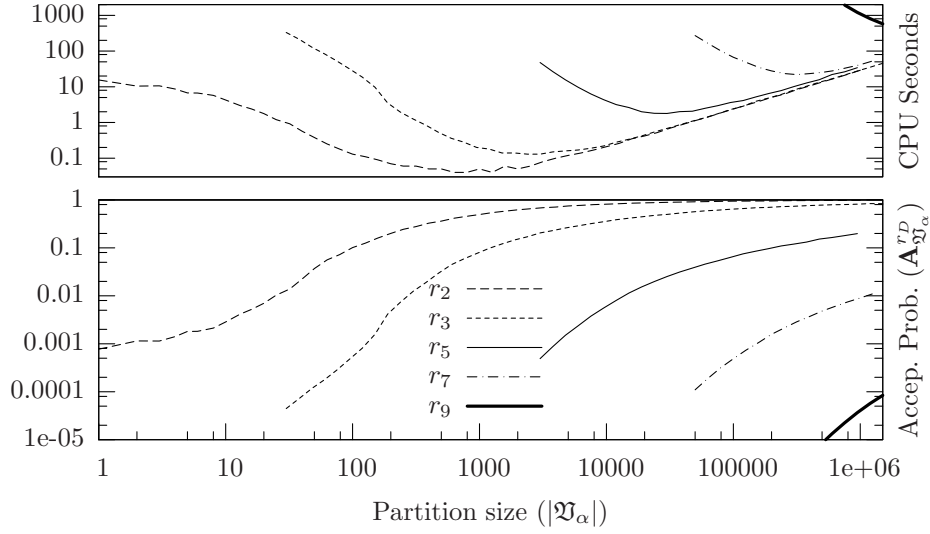


Fig. 8. Acceptance probability ($A_{\mathfrak{Y}_\alpha}^{r_D}$) and CPU time to generate 10^4 samples, as a function of partition size ($|\mathfrak{Y}_\alpha|$), for Rosenbrock targets r_D over $\Theta = [-10, 10]^{\otimes D}$, where D is the dimension.

Finally, we arrive at the infamous witch’s hat density which is considered to be a pathological target for most samplers [24]. The density is often thought of in two dimensions as an $m : (1 - m)$ mixture of a cone with center C and basal radius R and a uniform distribution on a rectangle. It can be easily generalized to D dimensions as follows:

$$w_r^D(X) = m \mathbf{1}_{\{\|X-C\| \leq R\}} \left(1 - \frac{\|X-C\|}{R} \right) H + (1 - m) \frac{1}{V}, \text{ where}$$

$$H = \frac{\Gamma(D/2)D(D+1)}{2\pi^{D/2}R^D}, \quad V = \prod_{i=1}^D d(\Theta_i), \quad R = 10^{-r}. \quad (12)$$

Our formulation of the witch’s hat is even more challenging than the differentiable formulation suggested in [24], as the gradient is 0 over the entire brim. MRS is amenable to any target with a well-defined interval extension over the domain including w_r^D . Mixtures of several sharply-peaked bivariate normals with a uniform distribution, a further generalization of the other formulation [24], pose no sampling problems to MRS. Figure 9 shows that one can efficiently sample from witch’s hat targets by rigorously constructing envelopes through the natural interval extension of (12). We can even sample from the hat of an eleven dimensional witch (w_0^{10}). We can also make the brim of the hat as large as $[-10^{100}, +10^{100}]^{\otimes 2}$ without much trouble (\hat{w}_0^2). Note that decreasing the radius has a similar effect as widening the brim, in terms of lowering the acceptance probability as a function of partition size. Note that we are able to sample rigorously from a range of multivariate witch’s hat targets with reasonable partition sizes and CPU seconds.

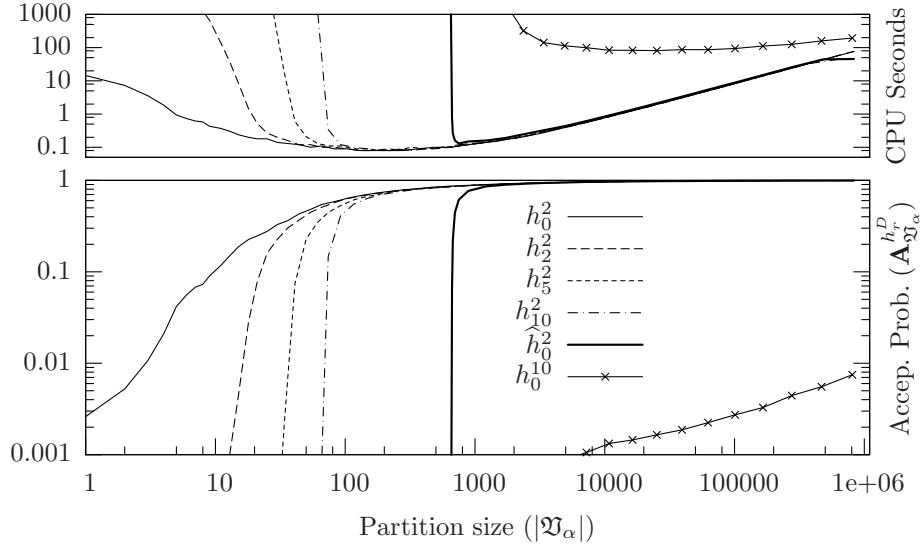


Fig. 9. Acceptance probability and CPU time to generate 10^4 samples, versus partition size for witch's hat targets w_r^D , where D is the dimension of the domain and $R = 10^{-r}$ is the hat's radius (12). The hats of all targets were centered at the two vector $(2, \dots, 2)$. The domain Θ for \hat{h}_0^2 was $[-10^{100}, +10^{100}]$, but all other targets had $\Theta = [-10, 10]^{\otimes D}$.

4.5. Likelihood of Jukes-Cantor Triplets and Quartets

Inferring the ancestral relationship among a set of species based on their DNA sequences is a basic problem in phylogenetics [40, 9]. One can obtain the likelihood of a particular phylogenetic tree that relates the species of interest by superimposing a simple Markov model of DNA substitution due to Jukes and Cantor [22] on that tree. The length of an edge (branch length) connecting two nodes (species) in the tree represents the amount of evolutionary time (divergence) between the two species. The likelihood function over trees obtained through a post-order traversal (e.g. [8]) has a natural interval extension over boxes of trees [39]. This allows us to draw samples from the posterior distribution over some compact box in the tree space using our MRS. Using the data from the mitochondria of Chimpanzee, Gorilla, and Orangutan [3] that can be summarized by 29 distinct site patterns [38], we obtain the posterior distribution by normalizing the likelihood with a uniform prior over the biologically meaningful compact domain $\Theta = [10^{-10}, 10]^{\otimes 3}$. 10,000 independent samples were drawn in 942 CPU seconds from the posterior distribution over Jukes-Cantor triplets, i.e. unrooted trees with three edges corresponding to the three primates emanating from their common ancestor. Figure 10 shows these samples (gray points) scattered about the verified global MLE of the triplet [39].

We were able to draw samples from Jukes-Cantor quartets (unrooted trees for four taxa) by adding the homologous sequence of the Gibbon which resulted in 61 distinct site patterns [38]. This is a more challenging problem because there are 3 distinct tree topologies for an unrooted quartet tree and each of these has five edges. Thus, the domain of quartets is a piecewise Euclidean space that arises from a fusion of 3 distinct five dimensional orthants. Since the post-order traversals specifying the likelihood function are topology-specific, we

extended the likelihood over a compact box of quartets in a topology-specific manner. The computational time was about a day and a half to draw 10,000 samples from the quartet target due to low acceptance probability of the naive likelihood function based on distinct site patterns. All the samples had the same topology which grouped Chimp and Gorilla together, i.e. ((Chimp, Gorilla), (Orangutan, Gibbon)). The samples were again scattered about the verified global MLE of the quartet [38]. The marginal triplet trees (dark dots) within the 10,000 sampled quartets are also plotted in Figure 10. Observe the influence of an additional taxon on the triplet estimates. This quartet likelihood function has an elaborate DAG (Definition 8) with numerous operations. When the data got compressed into sufficient statistic through algebraic statistical methods [36], the efficiency increased tremendously (for e.g. triplet efficiency increases by a factor of 3.7). This is due to the number of leaf nodes in the target DAG, which encode the distinct site patterns of the observed data into the likelihood function, getting reduced from 29 to 5 for the triplet target and from 61 to 15 for the quartet target [5]. Poor sampler efficiency makes it impractical to sample from trees with five or more leaves. However, one could use such triplets and quartets drawn from the posterior distribution to stochastically amalgamate and produce estimates of larger trees via fast amalgamating algorithms [41, 27]. A collection of large trees obtained through such stochastic amalgamations would account for the effect of finite sample sizes (sequence length) as well as the sensitivity of the amalgamating algorithm itself to variation in the input vector of small tree estimates. It would be interesting to investigate if such stochastic amalgamations can help improve mixing of MCMC algorithms on large tree spaces [35].

5. Conclusion

Interval methods provide a rigorous, efficient and fairly general way of constructing envelope functions for use in rejection sampling from target densities with a well-defined interval extension. In particular the method allows the envelope to be drawn from a large, flexible family of functions (simple functions over a family of adaptively refined partitions), and to be constructed in a manner that rigorously maintains the envelope property as the envelope function is adaptively refined. Refining the partition decreases the rejection probability at a rate that is no slower than linear with the mesh. The corresponding proposal density is easily constructed in $\mathcal{O}(\text{partition size})$ time into a data structure that allows samples from it to be drawn in constant time. When one substitutes conventional floating-point arithmetic for real arithmetic in a computer and uses discrete lattices to construct the envelope and/or proposal, it is generally not possible to guarantee the envelope property and thereby ensure that samples are drawn from the desired target density, except in special cases. For example, the adaptive rejection sampler (ARS) [16, 17] is efficient at drawing independent samples only from one dimensional log-concave targets. In ARS as well as a subsequent generalization of it through a Metropolis sampling step [18] to one dimensional non-log-concave targets, one can draw samples from higher dimensional targets by Gibbs sampling [14, 11] one dimension at a time. On one hand, Gibbs sampling, being a special case of Metropolis-Hastings sampling [6], is at the mercy of heuristic convergence diagnostics. On the other, proposals constructed for non-log-concave conditional densities from finitely many points cannot guarantee that the density has not soared between the sampled points. However, the construction of the Moore rejection sampler through interval methods, that enclose the target shape over the entire real continuum in any box of the domain

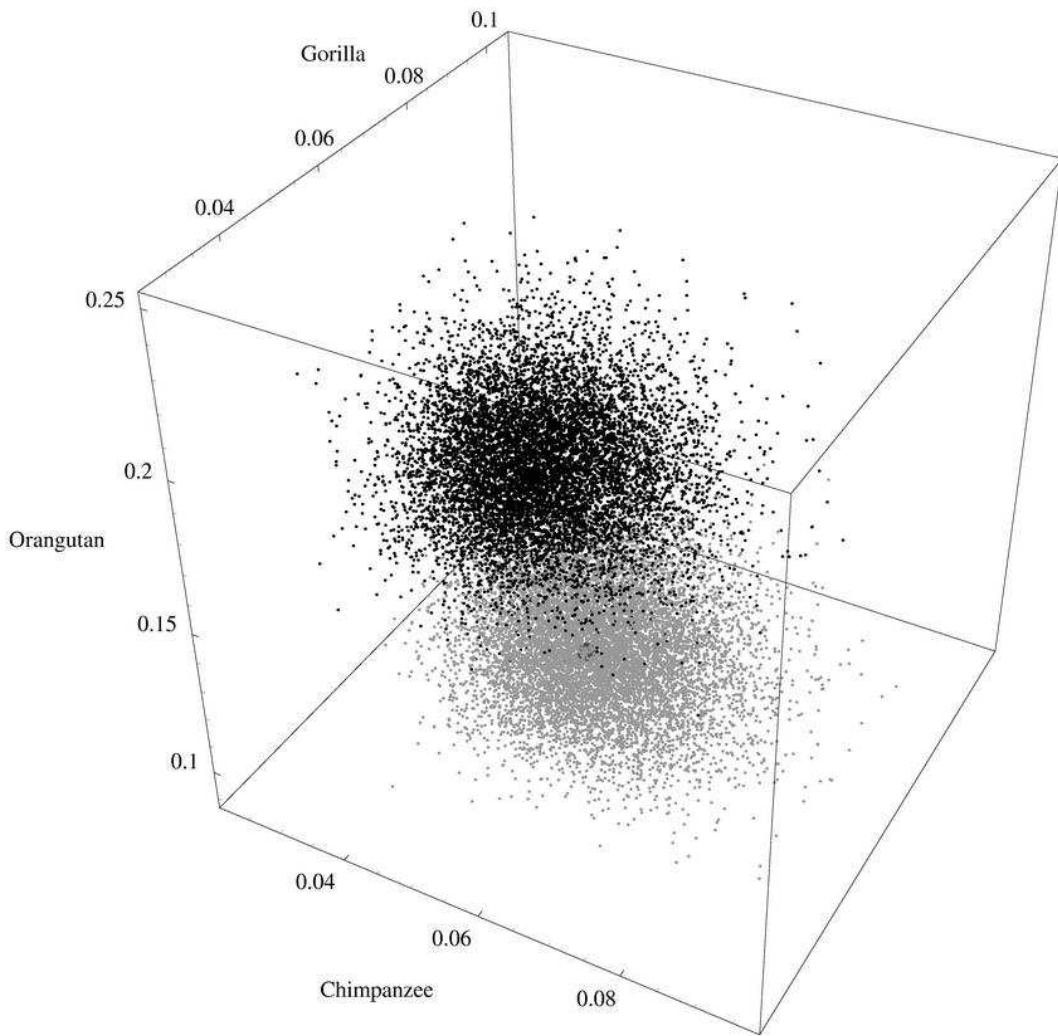


Fig. 10. 10,000 Moore rejection samples (gray dots) from the posterior distribution over the three branch lengths of the unrooted phylogenetic tree space of Chimpanzee, Gorilla and Orangutan based on their mitochondrial DNA. Marginal triplets (dark dots) of 10,000 samples from the quartet tree space of Chimp, Gorilla, Orangutan and Gibbon.

with machine-representable bounds, in a manner that rigorously accounts for all sources of numerical errors (see [25, 19] for a discussion on error control), naturally guarantees that the Moore rejection samples are independent draws from the desired target. Moreover, the target is allowed to be multivariate and/or non-log-concave with possibly ‘pathological’ behavior, as long as it has a well-defined interval extension.

Unfortunately, the efficiency of MRS is not immune to the curse of dimensionality and target DAG complexity. When the DAG for the likelihood gets large, its natural interval extension can have terrible over-enclosures of the true range, which in turn forces the adaptive refinement of the domain to be extremely fine for efficient envelope construction. Thus, a naive application of interval methods to targets with large DAGs can be terribly inefficient. In such cases, sampler efficiency rather than rigor is the issue. Thus, one will not obtain samples in a reasonable time rather than produce samples from some unknown and undesired target. There are several ways in which efficiency can be improved for such cases. First, the particular structure of the target DAG should be exploited to avoid any redundant computations. For example, algebraic statistical methods can be used to find sufficient statistics to dissolve symmetries in the DAG as done in Section 4.5. Second, we can further improve efficiency by limiting ourselves to differentiable targets in C^n . Tighter enclosures of the range $p^*(\Theta^{(i)})$ with $P^*(\Theta^{(i)})$ can come from the enclosures of Taylor expansions of p^* around the midpoint $m(\Theta^{(i)})$ through interval-extended automatic differentiation [37, 1, 25] that can then yield tighter estimates of the integral enclosures [42]. Third, we can employ pre-processing to improve efficiency. For example, we can pre-enclose the range of a possibly rescaled p^* over a partition of the domain and then obtain the enclosure of P^* over some arbitrary Θ through a combination of hash access and hull operations on the pre-enclosures. Such a pre-enclosing technique reduces not only the overestimation of target shapes with large DAGs but also the computational cost incurred while performing interval operations with processors that are optimized for floating-point arithmetic. Fourth, efficiency at the possible cost of rigor can also be gained (up to 30%) by foregoing directed rounding during envelope construction.

In this paper we focused on the interval extension of the simplest sampler, namely the rejection sampler. We also exploited the direct connections between rejection sampler, importance sampler and independent Metropolis-Hastings sampler to produce sample trios from the interval extensions of all three samplers. It would be interesting to compare other Monte Carlo methods to their natural interval extensions. For example, even Metropolis-coupled MCMC [15] which was designed to accelerate convergence for complicated targets is known to converge exponentially slowly in some cases [2]. Preliminary analysis suggests that a non-rigorous interval extension of the local Metropolis-Hastings sampler (relying on heuristic convergence diagnostics) may have a higher probability of converging to the target when compared to its floating-point cousin. Such hybrid samplers that rely on both interval and local methods may efficiently produce fairly reliable samples from challenging higher dimensional targets.

6. Acknowledgments

This was supported by a joint NSF/NIGMS grant DMS-02-01037 to Durrett, Aquadro, and Nielsen. R.S. is a Research Fellow of the Royal Commission for the Exhibition of 1851. Many thanks to Rob Strawderman and Warwick Tucker for constructive comments.

7. Appendix A

Arithmetic on intervals in $\mathbb{IR} \triangleq \{[x, y] : x \leq y, x, y \in \mathbb{R}\}$

DEFINITION 1 (INTERVAL ARITHMETIC). *If the binary operator \star is one of the elementary arithmetic operations $\{+, -, \cdot, /\}$, then we define an arithmetic on operands in \mathbb{IR} by*

$$X \star Y \triangleq \{x \star y : x \in X, y \in Y\}$$

with the exception that X/Y is undefined if $0 \in Y$.

THEOREM 1. *Arithmetic on the pair $X, Y \in \mathbb{IR}$ is given by:*

$$\begin{aligned} X + Y &= [\underline{x} + \underline{y}, \bar{x} + \bar{y}] \\ X - Y &= [\underline{x} - \bar{y}, \bar{x} - \underline{y}] \\ X \cdot Y &= [\min\{\underline{x}\underline{y}, \underline{x}\bar{y}, \bar{x}\underline{y}, \bar{x}\bar{y}\}, \max\{\underline{x}\underline{y}, \underline{x}\bar{y}, \bar{x}\underline{y}, \bar{x}\bar{y}\}], \\ X/Y &= X \cdot [1/\bar{y}, 1/\underline{y}], \text{ provided, } 0 \notin Y. \end{aligned}$$

Proof (cf. [19, 42]): Since any real arithmetic operation $x \star y$, where $\star \in \{+, -, \cdot, /\}$ and $x, y \in \mathbb{R}$, is a continuous function $x \star y \triangleq \star(x, y) : \mathbb{R} \times \mathbb{R} \rightarrow \mathbb{R}$, except when $y = 0$ under $/$ operation. Since X and Y are simply connected compact intervals, so is their product $X \times Y$. On such a domain $X \times Y$, the continuity of $\star(x, y)$ (except when $\star = /$ and $0 \in Y$) ensures the attainment of a minimum, a maximum and all intermediate values. Therefore, with the exception of the case when $\star = /$ and $0 \in Y$, the range $X \star Y$ has an interval form $[\min(x \star y), \max(x \star y)]$, where the min and max are taken over all pairs $(x, y) \in X \times Y$. Fortunately, we do not have to evaluate $x \star y$ over every $(x, y) \in X \times Y$ to find the global min and global max of $\star(x, y)$ over $X \times Y$, because the monotonicity of the $\star(x, y^*)$ in terms of $x \in X$ for any fixed $y^* \in Y$ implies that the extremal values are attained on the boundary of $X \times Y$, i.e., the set $\{\underline{x}, \underline{y}, \bar{x}, \bar{y}\}$. Thus the theorem can be verified by examining the finitely many boundary cases. \square

An extremely useful property of interval arithmetic that is a direct consequence of Definition 1 is summarized by the following theorem.

THEOREM 2 (FUNDAMENTAL PROPERTY OF INTERVAL ARITHMETIC). *If $X \subseteq X'$ and $Y \subseteq Y'$ and $\star \in \{+, -, \cdot, /\}$, then*

$$X \star Y \subseteq X' \star Y',$$

where we require that $0 \notin Y'$ when $\star = /$.

Proof:

$$X \star Y = \{x \star y : x \in X, y \in Y\} \subseteq \{x \star y : x \in X', y \in Y'\} = X' \star Y'. \square$$

Note that an immediate implication of Theorem 2 is that when $X = x$ and $Y = y$ are thin intervals (real numbers x and y), then $X' \star Y'$ will contain the result of the real arithmetic operation $x \star y$.

DEFINITION 2 (RANGE). *Consider a real-valued function $f : D \rightarrow \mathbb{R}$ where the domain $D \subseteq \mathbb{R}^n$. The range of f over any $E \subseteq D$ is represented by $\text{Rng}(f; E)$ and defined to be the set*

$$\text{Rng}(f; E) \triangleq \{f(x) : x \in E\}$$

However, when the range of f over any $X \in \mathbb{IR}^n$ such that $X \subseteq D$ is of interest, we will use the short-hand $f(X)$ for $\text{Rng}(f; X)$.

DEFINITION 3 (INTERVAL EXTENSION OF SUBSETS OF \mathbb{R}^n). For any Euclidean subset $\Theta \subseteq \mathbb{R}^n$ let us denote its interval extension by $\mathbb{I}\Theta$ and define it to be the set

$$\mathbb{I}\Theta \triangleq \{X \in \mathbb{IR}^n : \underline{x}, \bar{x} \in \Theta\}$$

We refer the the k th interval of interval vector or box $X \in \mathbb{IR}^n$ by X_k .

DEFINITION 4 (INCLUSION ISOTONY). An box-valued map $F : D \rightarrow \mathbb{IR}^m$, where $D \in \mathbb{IR}^n$, is inclusion isotonic if it satisfies the property

$$\forall X \subseteq Y \subseteq D \implies F(X) \subseteq F(Y).$$

DEFINITION 5 (THE NATURAL INTERVAL EXTENSION). Consider a real-valued function $f : D \rightarrow \mathbb{R}$ given by a formula, where the domain $D \in \mathbb{IR}^n$. If real constants, variables, and operations in f are replaced by their interval counterparts, then one obtains

$$F(X) : \mathbb{I}D \rightarrow \mathbb{IR}.$$

F is known as the natural interval extension of f . This extension is well-defined if we do not run into division by zero.

THEOREM 3 (INCLUSION ISOTONY OF RATIONAL FUNCTIONS). Consider the rational function $f(x) = p(x)/q(x)$, where p and q are polynomials. Let F be its natural interval extension such that $F(Y)$ is well-defined for some $Y \in \mathbb{IR}$ and let $X, X' \in \mathbb{IR}$. Then we have

- (i) Inclusion isotony: $\forall X \subseteq X' \subseteq Y \implies F(X) \subseteq F(X')$, and
- (ii) Range enclosure: $\forall X \subseteq Y \implies \text{Rng}(f; X) = f(X) \subseteq F(X)$.

Proof (cf. [42]): Since $F(Y)$ is well-defined, we will not run into division by zero, and therefore (i) follows from the repeated invocation of Theorem 2. We can prove (ii) by contradiction. Suppose $\text{Rng}(f; X) \not\subseteq F(X)$. Then there exists $x \in X$, such that $f(x) \in \text{Rng}(f; X)$ but $f(x) \notin F(X)$. This in turn implies that $f(x) = F([x, x]) \notin F(X)$, which contradicts (i). Therefore, our supposition cannot be true and we have proved (ii) $\text{Rng}(f; X) \subseteq F(X)$. \square

DEFINITION 6 (STANDARD FUNCTIONS). Piece-wise monotone functions, including exponential, logarithm, rational power, absolute value, and trigonometric functions, constitute the set of standard functions

$$\mathfrak{S} = \{a^x, \log_b(x), x^{p/q}, |x|, \sin(x), \cos(x), \tan(x), \sinh(x), \dots, \arcsin(x), \dots\}.$$

Such functions have well-defined interval extensions that satisfy inclusion isotony and *exact range enclosure*, i.e., $\text{Rng}(f; X) = f(X) = F(X)$. Consider the following definitions for the interval extensions for some monotone functions in \mathfrak{S} with $X \in \mathbb{IR}$,

$$\begin{aligned} \exp(X) &= [\exp(\underline{x}), \exp(\bar{x})] \\ \arctan(X) &= [\arctan(\underline{x}), \arctan(\bar{x})] \\ \sqrt{(X)} &= [\sqrt{(\underline{x})}, \sqrt{(\bar{x})}] && \text{if } 0 \leq \underline{x} \\ \log(X) &= [\log(\underline{x}), \log(\bar{x})] && \text{if } 0 < \underline{x} \end{aligned}$$

and a piece-wise monotone function in \mathfrak{S} with \mathbb{Z}^+ and \mathbb{Z}^- representing the set of positive and negative integers, respectively.

$$X^n = \begin{cases} [\underline{x}^n, \overline{x}^n] & : \text{if } n \in \mathbb{Z}^+ \text{ is odd,} \\ [(\langle X \rangle)^n, |X|^n] & : \text{if } n \in \mathbb{Z}^+ \text{ is even,} \\ [1, 1] & : \text{if } n = 0, \\ [1/\overline{x}, 1/\underline{x}]^{-n} & : \text{if } n \in \mathbb{Z}^-; 0 \notin X \end{cases}$$

DEFINITION 7 (ELEMENTARY FUNCTIONS). *A real-valued function that can be expressed as a finite combination of constants, variables, arithmetic operations, standard functions and compositions is called an elementary function. The set of all such elementary functions is referred to as \mathfrak{E} .*

DEFINITION 8 (DIRECTED ACYCLIC GRAPH (DAG) OF A FUNCTION). *One can think of the process by which an elementary function f is computed as the result of a sequence of recursive operations with the subexpressions f_i of f where, $i = 1, \dots, n < \infty$. This involves the evaluation of the subexpression f_i at node i with operands s_{i_1}, s_{i_2} from the sub-terminal nodes of i given by the directed acyclic graph (DAG) for f*

$$s_i = \odot f_i \triangleq \begin{cases} f_i(s_{i_1}, s_{i_2}) & : \text{if node } i \text{ has 2 sub-terminal nodes } s_{i_1}, s_{i_2} \\ f_i(s_{i_1}) & : \text{if node } i \text{ has 1 sub-terminal node } s_{i_1} \\ I(s_i) & : \text{if node } i \text{ is a leaf or terminal node, } I(x) = x. \end{cases} \quad (13)$$

The leaf or terminal node of the DAG is a constant or a variable and thus the f_i for a leaf i is set equal to the respective constant or variable. The recursion starts at the leaves and terminates at the root of the DAG. The DAG for an elementary f with n sub-expressions f_1, f_2, \dots, f_n is :

$$\{\odot f_i\}_{i=1}^n \rightsquigarrow \odot f_n = f(x), \quad (14)$$

where each $\odot f_i$ is computed according to (13).

For example the elementary function $x \cdot \sin((x-3)/3)$ can be obtained from the terminus $\odot f_6$ of the recursion $\{\odot f_i\}_{i=1}^6$ on the DAG for f as shown in Figure 11. It would be convenient if guaranteed enclosures of the range $f(X)$ of an elementary f can be obtained by its natural interval extension $F(X)$. We show that inclusion isotony does indeed hold for F , i.e. if $X \subseteq Y$, then $F(X) \subseteq F(Y)$, and in particular, the *inclusion property* that $x \in X \implies f(x) \in F(X)$ does hold.

THEOREM 4 (THE FUNDAMENTAL THEOREM OF INTERVAL ANALYSIS). *Consider any elementary function $f \in \mathfrak{E}$. Let $F : Y \rightarrow \mathbb{IR}$ be its natural interval extension such that $F(Y)$ is well-defined for some $Y \in \mathbb{IR}$ and let $X, X' \in \mathbb{IR}$. Then we have*

- (i) Inclusion isotony: $\forall X \subseteq X' \subseteq Y \implies F(X) \subseteq F(X')$, and
- (ii) Range enclosure: $\forall X \subseteq Y \implies \text{Rng}(f; X) = f(X) \subseteq F(X)$.

Proof (cf. [42]): Any elementary function $f \in \mathfrak{E}$ is defined by the recursion 14 on its sub-expressions f_i where $i \in \{1, \dots, n\}$ according to its DAG. If $f(x) = p(x)/q(x)$ is a rational function, then the theorem already holds by Theorem 3, and if $f \in \mathfrak{S}$ then the theorem

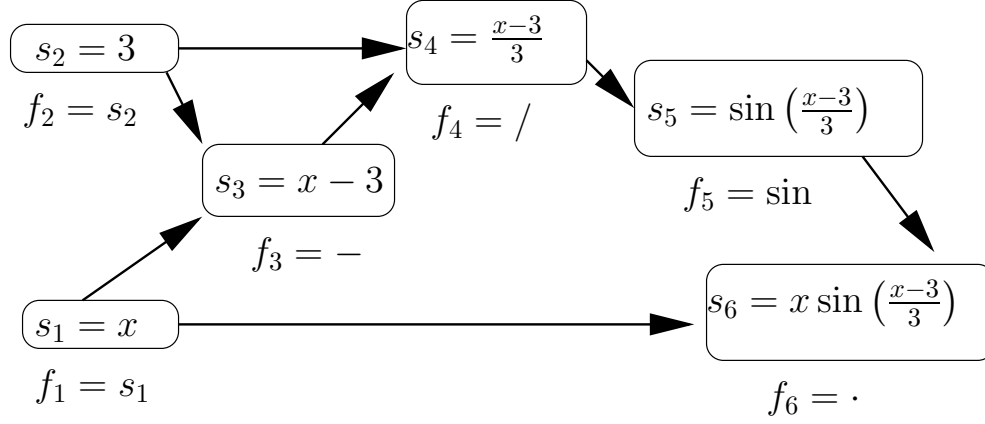


Fig. 11. Recursive evaluation of the sub-expressions f_1, \dots, f_6 on the DAG of the elementary function $f(x) = \odot f_6 = x \cdot \sin((x-3)/3)$

holds because the range enclosure is exact for standard functions. Thus it suffices to show that if the theorem holds for $f_1, f_2 \in \mathfrak{E}$, then the theorem also holds for $f_1 \star f_2$, where $\star \in \{+, -, /, \cdot, \circ\}$. By \circ we mean the composition operator. Since the proof is analogous for all five operators, we only focus on the \circ operator. Since F is well-defined on its domain Y , neither the real-valued f nor any of its sub-expressions f_i have singularities in its respective domain Y_i induced by Y . In particular f_2 is continuous on any X_2 and X'_2 such that $X_2 \subseteq X'_2 \subseteq Y_2$ implying the compactness of $F_2(X_2) \triangleq W_2$ and $F_2(X'_2) \triangleq W'_2$, respectively. By our assumption that F_1 and F_2 are inclusion isotonic we have that $W_2 \subseteq W'_2$ and also that

$$F_1 \circ F_2(X_2) = F_1(F_2(X_2)) = F_1(W_2) \subseteq F_1(W'_2) = F_1(F_2(X'_2)) = F_1 \circ F_2(X_2)$$

The range enclosure is a consequence of inclusion isotony by an argument identical to that given in the proof for Theorem 3. \square

The fundamental implication of the above theorem is that it allows us to enclose the range of any elementary function and thereby produces an upper bound for the global maximum and a lower bound for the global minimum over any compact subset of the domain upon which the function is well-defined. We will see in the sequel that this is the work-horse of randomized enclosure algorithms that efficiently produce samples even from highly multi-modal target distributions.

Unlike the natural interval extension of an $f \in \mathfrak{S}$ that produces exact range enclosures, the natural interval extension $F(X)$ of an $f \in \mathfrak{E}$ often overestimates the range $f(X)$, but can be shown under mild conditions to linearly approach the range as the maximal diameter of the box X goes to zero, i.e., $\mathfrak{h}(F(X), f(X)) \leq \alpha \cdot d_\infty(X)$ for some $\alpha \geq 0$. This implies that a partition of X into smaller boxes $\{X^{(1)}, \dots, X^{(m)}\}$ gives better enclosures of $f(X)$ through the union $\bigcup_{i=1}^m F(X^{(i)})$ as illustrated in Figure 12. Next we make the above statements precise.

DEFINITION 9. A function $f : D \rightarrow \mathbb{R}$ is Lipschitz if there exists a Lipschitz constant K such that, for all $x, y \in D$, we have $|f(x) - f(y)| \leq K|x - y|$. We define \mathfrak{E}_L to be

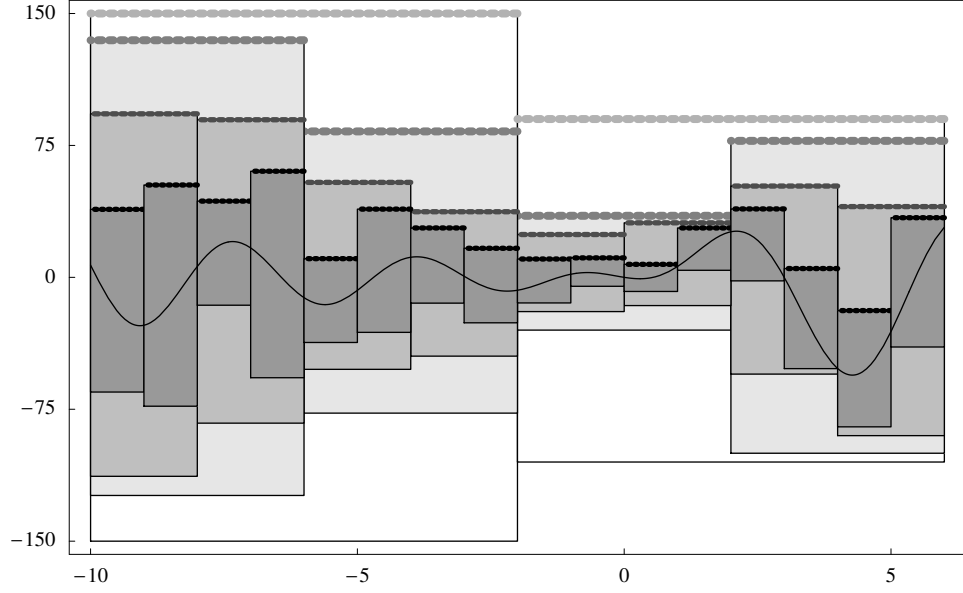


Fig. 12. Range enclosure of the interval extension of $-\sum_{k=1}^5 k x \sin\left(\frac{k(x-3)}{3}\right)$ linearly tightens with the mesh.

the set of elementary functions whose sub-expressions f_i , $i = 1, \dots, n$ at the nodes of the corresponding DAGs are all Lipschitz.

THEOREM 5 (RANGE ENCLOSURE TIGHTENS LINEARLY WITH MESH). Consider a function $f : D \rightarrow \mathbb{R}$ with $f \in \mathfrak{E}_{\mathcal{G}}$. Let F be an inclusion isotonic interval extension of f such that $F(X)$ is well-defined for some $X \in \mathbb{IR}$, $X \subseteq I$. Then there exists a positive real number K , depending on F and X , such that if $X = \cup_{i=1}^k X^{(i)}$, then

$$\text{Rng}(f; X) \subseteq \bigcup_{i=1}^k F(X^{(i)}) \subseteq F(X)$$

and

$$r\left(\bigcup_{i=1}^k F(X^{(i)})\right) \leq r(\text{Rng}(f; X)) + K \max_{i=1, \dots, k} r(X^{(i)})$$

Proof : The proof is given by an induction on the DAG for f similar to the proof of Theorem 4 (See [42]).

8. Appendix B

Here we will study the Moore rejection sampler (MRS) carefully. Lemma 1 shows that MRS indeed produces independent samples from the desired target and Lemma 2 describes the asymptotics of the acceptance probability as the partition of the domain is refined.

LEMMA 1. Suppose that the target shape p^* has a well-defined natural interval extension P^* . If U is generated according to the steps in part c of the rejection sampling algorithm, and if the proposal density $q^{\bar{x}}(\theta)$ and the envelope function $f_{q^{\bar{x}}}(\theta)$ are given by (4) and (5), respectively, then U is distributed according to the target p .

Proof: From (4) and (5) observe that $f_{q^{\bar{x}}}(t) = q^{\bar{x}}(t)N_{q^{\bar{x}}}$. Let us define the following two subsets of \mathbb{R}^2 ,

$$\mathcal{B}_q = \{(t, h) : 0 \leq h \leq f_{q^{\bar{x}}}(t)\}, \text{ and } \mathcal{B}_p = \{(t, h) : 0 \leq h \leq p^*(t)\}.$$

First let us agree that steps ci and cii of part c of the rejection sampling algorithm produce a pair (T, H) that is uniformly distributed on \mathcal{B}_q . We can see this by letting $k(t, h)$ denote the joint density of (T, H) and $k(h|t)$ denote the conditional density of H given $T = t$. Then,

$$k(t, h) = \begin{cases} q^{\bar{x}}(t) k(h|t) & \text{if } (t, h) \in \mathcal{B}_q \\ 0 & \text{otherwise.} \end{cases}$$

Since we sample a uniform height h for a given t in Step cii of the algorithm

$$k(h|t) = \begin{cases} (f_{q^{\bar{x}}}(t))^{-1} = (q^{\bar{x}}(t)N_{q^{\bar{x}}})^{-1} & \text{if } h \in [0, f_{q^{\bar{x}}}(t)] \\ 0 & \text{otherwise.} \end{cases}$$

Therefore,

$$k(t, h) = \begin{cases} q^{\bar{x}}(t) k(h|t) = q^{\bar{x}}(t)/(q^{\bar{x}}(t)N_{q^{\bar{x}}}) = (N_{q^{\bar{x}}})^{-1} & \text{if } (t, h) \in \mathcal{B}_q \\ 0 & \text{otherwise.} \end{cases}$$

Thus we have shown that the joint density of (T, H) is a uniform distribution on \mathcal{B}_q . The above relationship also makes geometric sense since the volume of \mathcal{B}_q is exactly $N_{q^{\bar{x}}}$. Now, let (T^*, H^*) be an accepted point, i.e., $(T^*, H^*) \in \mathcal{B}_p \subseteq \mathcal{B}_q$. Then, the uniform distribution of (T, H) on \mathcal{B}_q implies the uniform distribution of (T^*, H^*) on \mathcal{B}_p . Since the volume of \mathcal{B}_p is N_p , the p.d.f. of (T^*, H^*) is identically $1/N_p$ on \mathcal{B}_p and 0 elsewhere. Hence, the marginal p.d.f. of $U = T^*$ is

$$\begin{aligned} w(u) &= \int_0^{p^*(u)} 1/N_p dh \\ &= 1/N_p \int_0^{p^*(u)} 1 dh \\ &= 1/N_p \int_0^{N_p p(u)} 1 dh, \quad \because p(u) = p^*(u)/N_p \\ &= p(u). \quad \square \end{aligned}$$

LEMMA 2. Let \mathcal{U}_W be the uniform partition of $\Theta = [\underline{\theta}, \bar{\theta}]$ into W intervals each of diameter w

$$\begin{aligned} w &= \frac{\bar{\theta} - \underline{\theta}}{W} \\ \Theta_W^{(i)} &= [\underline{\theta} + (i-1)w, \underline{\theta} + iw], i = 1, \dots, W \\ \mathcal{U}_W &= \{\Theta_W^{(i)}, i = 1, \dots, W\}. \end{aligned}$$

and let $p^* \in \mathfrak{E}_{\mathcal{L}}$, then

$$\mathbf{A}_{\mathcal{U}_W}^p = 1 - \mathcal{O}(1/W)$$

Proof

Then by means of Theorem 5

$$\begin{aligned} d(\Theta_W^{(i)}) = \mathcal{O}(1/W) &\implies \mathfrak{h}(p^*(\Theta_W^{(i)}), P^*(\Theta_W^{(i)})) = \mathcal{O}(1/W) \\ &\implies d(P^*(\Theta_W^{(i)})) = \mathcal{O}(1/W), \quad \because p^* \in \mathfrak{E}_{\mathfrak{L}} \end{aligned}$$

Therefore

$$\sum_{i=1}^{|\mathfrak{U}_W|} \left(d(\Theta_W^{(i)}) \cdot P^*(\Theta_W^{(i)}) \right) = w \sum_{i=1}^W P^*([\underline{\theta} + (i-1)w, \underline{\theta} + iw]),$$

and we have

$$d(w \sum_{i=1}^W P^*(\Theta_W^{(i)})) = \mathcal{O}(1/W) \implies \mathbf{A}_{\mathfrak{U}_W}^p = 1 - \mathcal{O}(1/W)$$

Therefore the lower bound for the acceptance probability $\mathbf{A}_{\mathfrak{U}_W}^p$ of MRS approaches 1 no slower than linearly with the refinement of Θ by \mathfrak{U}_W . Note that this should hold for a general nonuniform partition with w replaced by the mesh. \square

References

- [1] M Berz. Forward algorithms for high orders and many variables with application to beam physics. In A Griewank and G Corliss, editors, *Automatic differentiation of algorithms: theory, implementation and applications*, pages 147–156. SIAM, 1991.
- [2] N Bhatnagar and D Randall. Torpid mixing of simulated tempering on the Potts model. In *Proceedings of the 15th annual ACM-SIAM symposium on discrete algorithms (SODA)*, pages 478–487. New Orleans, LA, 2004.
- [3] WM Brown, EM Prager, A Wang, and AC Wilson. Mitochondrial DNA sequences of primates, tempo and mode of evolution. *Journal of Molecular Evolution*, 18:225–239, 1982.
- [4] H Cai. Exact sampling using auxiliary variables. Preprint, University of Missouri - St. Louis, 1999.
- [5] M Casanellas, LD Garcia, and S Sullivant. Catalog of small trees. In L Pachter and B Sturmfels, editors, *Algebraic statistics for computational biology*, pages 291–304. Cambridge University Press, 2005.
- [6] S Chib and E Greenberg. Understanding the Metropolis-Hastings algorithm. *The American Statistician*, 49:327–335, 1995.
- [7] P. Diaconis and L. Saloff-Coste. What do we know about the metropolis algorithm ? *Jnl. Comp. Sys. Sci.*, 57:20–36, 1998.
- [8] J Felsenstein. Evolutionary trees from DNA sequences: a maximum likelihood approach. *Journal of Molecular Evolution*, 17:368–376, 1981.
- [9] J. Felsenstein. *Inferring phylogenies*. Sinauer Associates, Sunderland, MA, 2003.
- [10] M Galassi, J Davies, J Theiler, B Gough, G Jungman, M Booth, and F Rossi. *GNU Scientific Library Reference Manual - Second Edition*. Network Theory Ltd., 2003.
- [11] AE Gelfand and AFM Smith. Sampling-based approaches to calculating marginal densities. *Jnl. Am. Statist. Ass.*, 85:398–409, 1990.
- [12] A Gelman. Inference and monitoring convergence. In WR Gilks, S Richardson, and DJ Spiegelhalter, editors, *Markov Chain Monte Carlo in Practice*, page 137. Chapman and Hall, 1996.
- [13] A Gelman and DB Rubin. Inference from iterative simulation using multiple sequences (with duscussion). *Statistical Science*, 7:457–511, 1992.
- [14] S Geman and D Geman. Stochastic relaxation, Gibbs distribution and the Bayesian restoration of images. *IEEE Trans. Pattn. Anal. Mach. Intell.*, 6:721–741, 1984.
- [15] CG Geyer. Markov chain Monte Carlo maximum likelihood. In *Computer science and statistics: proceedings of the 23rd symposium interface*, pages 156–163. Interface foundation, 1991.

- [16] WR Gilks. Derivative-free adaptive rejection sampling for gibbs sampling. In J Bernardo, J Berger, AP Dawid, and AFM Smith, editors, *Bayesian Statistics 4*. Oxford Univ. Press, 1992.
- [17] WR Gilks, NG Best, and KKC Tan. Adaptive rejection sampling for Gibbs sampling. *Applied Statistics*, 41:337–348, 1992.
- [18] WR Gilks, NG Best, and KKC Tan. Adaptive rejection metropolis sampling. *Applied Statistics*, 44:455–472, 1995.
- [19] R Hammer, M Hocks, U Kulisch, and D Ratz. *C++ toolbox for verified computing: basic numerical problems*. Springer-Verlag, 1995.
- [20] W Hastings. Monte Carlo sampling methods using markov chains and their applications. *Biometrika*, 57:97–109, 1970.
- [21] Hofschuster and Krämer. C-XSC 2.0: A C++ library for extended scientific computing. In R Alt, A Frommer, RB Kearfott, and W Luther, editors, *Numerical software with result verification*, volume 2991 of *Lecture notes in computer science*, pages 15–35. Springer-Verlag, 2004.
- [22] TH Jukes and C Cantor. Evolution of protein molecules. In HN Munro, editor, *Mammalian Protein Metabolism*, pages 21–32. New York Academic Press, 1969.
- [23] H Kahn and AW Marshall. Methods of reducing sample size in Monte Carlo computations. *Journal of the Operational Research Society of America*, 1:263–271, 1953.
- [24] RE Kass, BP Carlin, A Gelman, and RM Neal. Markov chain Monte Carlo in practice: a round table discussion. *The American Statistician*, 52:93–100, 1998.
- [25] U Kulisch. Advanced arithmetic for the digital computer, interval arithmetic revisited. In U Kulisch, R Lohner, and A Facius, editors, *Perspectives on enclosure methods*, pages 50–70. Springer-Verlag, 2001.
- [26] U Kulisch, R Lohner, and A Facius, editors. *Perspectives on enclosure methods*. Springer-Verlag, 2001.
- [27] D Levy, R Yoshida, and L Pachter. Beyond pairwise distances: Neighbor joining with phylogenetic diversity estimates. *Mol. Biol. Evol.*, Advance Access published on November 9, 2005.
- [28] J Liu. Metropolisised independent sampling and comparisons to rejection sampling and importance sampling. *Statist. and Comput.*, 6:113–119, 1995.
- [29] N Madras. *Lecture notes on Monte Carlo methods*. American Mathematical Society, 2002.
- [30] G Marsaglia. Generating discrete random numbers in a computer. *Comm ACM*, 6:37–38, 1963.
- [31] AW Marshall. The use of multi-stage sampling schemes in Monte Carlo computation. In M Meyer, editor, *Symposium on Monte Carlo methods*, pages 123–140. Wiley, 1956.

- [32] M Matsumoto and T Nishimura. Mersenne twister: A 623-dimensionally equidistributed uniform pseudo-random number generator. *ACM Trans. Model. Comput. Simul.*, 8(1):3–30, 1998.
- [33] N Metropolis, A Rosenbluth, M Rosenbluth, A Teller, and E Teller. Equations of state calculations by fast computing machines. *Jnl. Chem. Phys.*, 21:1087–1092, 1953.
- [34] RE Moore. *Interval analysis*. Prentice-Hall, 1967.
- [35] E Mossel and E Vigoda. Phylogenetic MCMC algorithms are misleading on mixtures of trees. *Science*, 309:2207–2209, 2005.
- [36] L Pachter and B Sturmfels, editors. *Algebraic statistics for computational biology*. Cambridge University Press, 2005.
- [37] LB Rall. *Automatic differentiation, techniques and applications*, volume 120 of *Springer lecture notes in computer science*. Springer-Verlag, 1981.
- [38] R Sainudiin. Enclosing the maximum likelihood of the simplest DNA model evolving on fixed topologies: towards a rigorous framework for phylogenetic inference. Technical Report BU1653-M, Department of Biol. Stats. and Comp. Bio., Cornell University, 2004.
- [39] R Sainudiin and R Yoshida. Applications of interval methods to phylogenetic trees. In L Pachter and B Sturmfels, editors, *Algebraic statistics for computational biology*, pages 359–374. Cambridge University Press, 2005.
- [40] C Semple and M Steel. *Phylogenetics*. Oxford University Press, 2003.
- [41] K Strimmer and A von Haeseler. Quartet puzzling: A quartet maximum likelihood method for reconstructing tree topologies. *Mol. Biol. Evol.*, 13:964–969, 1996.
- [42] W Tucker. Auto-validating numerical methods. Lecture notes, Uppsala University, 2004.
- [43] J von Neumann. Various techniques used in connection with random digits. In *John Von Neumann, Collected Works*, volume V. Oxford University Press, 1963.
- [44] AJ Walker. An efficient method for generating discrete random variables with general distributions. *ACM Trans on Mathematical Software*, 3:253–256, 1977.
- [45] D Williams. *Weighing the Odds: A Course in Probability and Statistics*. Cambridge University Press, 2001.